Published in final edited form as:
J Neurosci. 2011 November 16; 31(46): 16814–16825. doi:10.1523/JNEUROSCI.3064-11.2011.

HCN Channels Expressed in the Inner Ear Are Necessary for Normal Balance Function

Geoffrey C. Horwitz[1], **Jessica R. Risner-Janiczek**[1], **Sherri M. Jones**[3], and **Jeffrey R. Holt**[1,2]

[1]Department of Neuroscience, University of Virginia School of Medicine, P.O. Box 801392, Charlottesville, Virginia 22908, USA.

[2]Department of Otolaryngology, University of Virginia School of Medicine, P.O. Box 801392, Charlottesville, Virginia 22908, USA.

[3]Department of Communication Sciences and Disorders, East Carolina University, Greenville, North Carolina 27858, USA.

Abstract

HCN1-4 subunits form Na^+/K^+ permeable ion channels that are activated by hyperpolarization and carry the current known as I_h. I_h has been characterized in vestibular hair cells of the inner ear, but its molecular correlates and functional contributions have not been elucidated. We examined *Hcn* mRNA expression and immunolocalization of HCN protein in the mouse utricle, a mechanosensitive organ that contributes to the sense of balance. We found that HCN1 is the most highly expressed subunit, localized to the basolateral membranes of type I and type II hair cells. We characterized I_h using the whole-cell, voltage-clamp technique and found the current expressed in ~90% of the cells with a mean maximum conductance of 4.4 nS. I_h was inhibited by ZD7288, Cilobradine and by adenoviral expression of a dominant-negative form of HCN2. To determine which HCN subunits carried I_h we examined hair cells from mice deficient in *Hcn1, 2,* or both. I_h was completely abolished in hair cells of $Hcn1^{-/-}$ mice and $Hcn1,2^{-/-}$ mice but was similar to wild-type in $Hcn2^{-/-}$ mice. To examine the functional contributions of I_h, we recorded hair cell membrane responses to small hyperpolarizing current steps and found that activation of I_h evoked a 5-10 mV sag depolarization and a subsequent 15-20 mV rebound upon termination. The sag and rebound were nearly abolished in *Hcn1*-deficient hair cells. We also found that *Hcn1*-deficient mice had deficits in vestibular evoked potentials and balance assays. We conclude that HCN1 contributes to vestibular hair cell function and the sense of balance.

Keywords

HCN; HCN1; hair cell; utricle; vestibular; I_h

INTRODUCTION

Encoding head movement into sensory information by the vestibular system is initiated by cation influx through transduction channels at the apical pole of mechanosensory hair cells. The information is transmitted at the basal pole by release of glutamate at the hair cell afferent synapse. Between the two poles resides a variety of ion channels that shape graded receptor potentials as they propagate from apex to base. Because the hair cell response is graded, small changes in ion channel activity influence membrane potential, calcium

Correspondence should be addressed to: Jeffrey R. Holt, Ph.D. Department of Otolaryngology, Children's Hospital Boston Harvard Medical School 300 Longwood Avenue, CLS 12251 Boston, MA 02115 Jeffrey.Holt@Childrens.Harvard.Edu Tel: 617-919-3574.

channel open probability, and neurotransmitter release. The precise contributions of hair cell ion channels to sensory processing in the vestibular system and to the sense of balance are poorly understood. Here we investigate the contributions of the *Hcn* gene family, which encodes ion channels that are active around the hair cell resting potential.

The *Hcn* family consists of four members, *Hcn1-4* (Santoro et al., 1998; Ludwig et al., 1998), which encode subunits that form homo- or hetero-tetrameric ion channels (Much et al., 2003). HCN channels are activated by hyperpolarization and carry currents known as I_f, I_Q, or, as referred to here, I_h. I_h is unusual as it activates at potentials negative to -40 mV, is carried by both Na^+ and K^+, and is sensitive to cyclic nucleotides (Biel et al., 2009). The current was first identified in cardiac tissue (Noma and Irisawa, 1976; Brown et al., 1979; DiFrancesco, 1981), but is also present in both central and peripheral neurons (Fain et al., 1978; Bader et al., 1979; Halliwell and Adams, 1982). I_h has been identified in a number of sensory systems including the visual, auditory and vestibular systems. In the retina, I_h is crucial for rod bipolar cells, a sensory cell with graded receptor potentials (Cangiano et al., 2007). Within the inner ear, I_h has been characterized in vestibular (Chabbert et al., 2001) and auditory neurons (Mo and Davis, 1997; Yi et al., 2010), as well as in vestibular hair cells (Holt and Eatock, 1995; Rüsch et al., 1998), but its molecular composition and functional contributions are unclear.

In a previous study we examined the contributions of the *Hcn* gene family in sensory hair bundles but found that HCN channels are not required for hair cell mechanotransduction (Horwitz et al., 2010). For the present study we examine the contributions of HCN subunits to basolateral conductances in vestibular hair cells. We use quantitative PCR and immunolocalization to examine expression of *Hcn* mRNA and protein, respectively. We characterize the development and biophysical properties of I_h in postnatal mouse vestibular hair cells. We show that the current is mildly sensitive to cAMP, can be blocked by ZD7288 or Cilobradine, and is inhibited by exogenous expression of a form of HCN2 that carries a dominant-negative pore mutation. We examine *Hcn1*-, *Hcn2*-, and *Hcn1,2*- deficient mice and find that I_h is carried primarily by HCN1 in vestibular hair cells. We find that loss of I_h results in deficits in hair cell voltage responses, particularly for small current steps. Vestibular evoked potentials have reduced amplitudes in *Hcn1*-deficient mice suggesting asynchronous activity in the 8th cranial nerve. Lastly, mice that lack *Hcn1* perform poorly on rotarod tasks indicating *Hcn1* is required for normal balance function.

MATERIALS AND METHODS

Animals

All animal protocols were approved by the Animal Care and Use Committee at the University of Virginia (Protocol #3123). Nine mouse genotypes were used for this study. We did not differentiate between genders, and approximately equal numbers of males and females were used. Swiss Webster mice (Hilltop Lab Animals Inc., Scottsdale, PA and Taconic Farms, Germantown, NY) and B6129SF2/J mice (The Jackson Laboratory, Bar Harbor, ME) were used as control mice. *Hcn1* $^{-/-}$ mice (B6;129-HCN1^{tm2Kndl}/J) were generated as previously described (Nolan et al., 2003) and were obtained from The Jackson Laboratory. *Hcn2*$^{-/-}$ mice were obtained from Ludwig et al. (2003). *Hcn1/2* double knockout mice were created from crosses of *Hcn1*$^{-/-}$ and *Hcn2*$^{+/-}$ mice. *Hcn1*$^{+/-}$*; Hcn2*$^{+/-}$ mice were created and crossed, which gave rise to *Hcn1/2*$^{-/-}$ mice. Mice that carried a floxed allele of *Hcn1* (*Hcn1*$^{f/+}$) were obtained from Nolan et al. (2003). These mice were crossed with mice that targeted Cre recombinase to the *Foxg1* locus (Hebert and McConnell, 2000). *Hcn1*$^{f/+}$ mice with *Foxg1-Cre recombinase* were crossed to produce both *Hcn1*$^{f/f}$ mice expressing Cre and *Hcn1*$^{f/f}$ mice without Cre. Floxed mice were also crossed with global knocks to create *Hcn1*$^{f/-}$ mice. No differences in currents or behavior were observed

between *Hcn1*$^{f/f}$ and *Hcn1*$^{f/-}$ mice, therefore data from these mice were pooled during analysis. H*cn1*$^{+/+}$ mice expressing *Foxg1-Cre recombinase* were also used in some control experiments.

Tissue preparation

The mouse utricle sensory epithelium was harvested at postnatal day (P) 0 to P25 as previously described (Holt et al., 1997). Briefly, mouse pups were killed by rapid decapitation and the temporal bones were excised and bathed in MEM with Glutamax (Invitrogen, Carlsbad, CA) supplemented with 10 mM HEPES and 0.05 mg/mL Ampicillin (pH 7.4). The utricle sensory epithelium was gently dissected and mounted on a glass coverslip beneath a pair of thin glass fibers glued to the coverslip to stabilize the tissue in a flat position.

Quantitative PCR

Total RNA was isolated as described previously (Horwitz et al., 2010) from the sensory epithelium of utricles acutely excised from B6129SF2/J mice. RNA concentration was measured on a spectrophotometer (Nandodrop, ND100, Thermo Fisher Scientific, Pittsburgh, PA). To insure the quality of isolated RNA, samples were analyzed with a Bioanalyzer (Agilent Technologies, Santa Clara, CA) and found to have an RNA integrity number of >8.0. RNA was reverse transcribed into cDNA. Quantitative PCR primers were designed using the PrimerQuest Software from Integrated DNA Technologies (San Diego, CA). Primers were designed with melting temperatures near 61°C. The primer sequences were: *Hcn1* – ACATGCTGTGCATTGGTTATGGCG and AACAAACATTGCGTAGCAGGTGGC; *Hcn2* – ACTTCCGCACCGGCATTGTTATTG and TCGATTCCCTTCTCCACTATG AGG; *Hcn3* – CCTCATCCGCTACATACACCAGT and GACACAGCAGCAACATC ATTCC; *Hcn4* – GCATGATGCTTCTGCTGTGTCACT and TTCACCATGCCATTGATGGACACC. Each sequence was designed to amplify a region within the amplicon produced from RT-PCR described in Horwitz et al. (2010), and was screened using a BLAST inquiry to verify specificity. Single-color quantitative PCR reactions were designed and carried out in triplicate according to manufacturer specifications using iQ SYBR Green Supermix (BioRad, Hercules, CA) and run on an iCycler (BioRad, Hercules, CA). Amplicons were generated for 40 cycles, and specificity was confirmed using melt curve analysis.

Expression ratios were calculated by comparing C_t generated from each HCN subunit primer set. Thresholds were normalized to housekeeping gene 29S, and efficiencies of each primer set were confirmed through generation of standard curves as described previously (Horwitz et al., 2010).

Immunohistochemistry

Utricles were excised from B6129SF2/J (The Jackson Laboratory, Bar Harbor, ME), Swiss Webster (Taconic Farms, Germantown, NY), B6;129-HCN1^{tm2Kndl}/J (The Jackson Laboratory) mouse pups between P4 and P9. The epithelia were placed on glass coverslips under two glass fibers and were bathed in MEM with Glutamax (Invitrogen, Carlsbad, CA) buffered with 10mM HEPES (Sigma, St. Louis, MO). The tissue was then placed in fixative containing 4% paraformaldehyde in 0.1 M phosphate buffered saline (PBS) for 15-20 minutes. Following fixation, the tissue was rinsed in PBS, incubated in 0.1% TritonX100 for 15 minutes, and blocked for one hour using a 3% bovine serum albumin and normal donkey serum. Incubation with primary antibodies was done overnight at 4°C. For HCN1, we used a goat polyclonal antibody directed against the C-terminus (Santa Cruz, Santa Cruz, CA, sc-19706, 1:50 dilution). For HCN2 and HCN4 the primary antibodies were rabbit polyclonal directed against the N-terminus (Alomone, Israel, APC-030, 1:100 dilution and

APC-052, 1:200 dilution). We used antibodies directed against Myosin 7a (Proteus Biosciences, Ramona, CA, 1:1000 dilution) and Neurofilament (Sigma, 1:4000 dilution) as markers for hair cells and calyx terminals respectively. The tissue was then incubated with Alexa Fluor secondary antibodies and phalloidin (Invitrogen, Carlsbad, CA). Samples were imaged using a 63x objective on a Zeiss LSM510 confocal microscope (Oberkochen, Germany). Three-dimensional projection images were created following Z-series acquisition using the Zeiss LSM Image Browser.

Electrophysiological recording

Recordings were performed in standard artificial perilymph solution containing (in mM): 144 NaCl, 0.7 NaH_2PO_4, 5.8 KCl, 1.3 $CaCl_2$, 0.9 $MgCl_2$, 5.6 D-glucose, and 10 HEPES-NaOH, adjusted to pH 7.4 and 320 mOsmol/kg. Vitamins (1:50; Cat #11120) and amino acids (1:100; Cat #11130) were added from concentrates (Invitrogen, Carlsbad, CA). Pharmacology was assayed using bath application of $BaCl_2$ (Sigma), ZD7288 (Tocris), Cilobradine (DK-AH-269, Sigma), and 8-Br-cAMP (Sigma). Hair cells were viewed from the apical surface using an upright Axioskop FS microscope (Zeiss, Oberkochen, Germany) equipped with a 63X water immersion objective with differential interference contrast optics. Recording pipettes (3-5 MΩ) were pulled from R6 capillary glass (King Precision Glass, Claremont, CA) and filled with intracellular solution containing (in mM): 135 KCl, 5 EGTA-KOH, 5 HEPES, 2.5 K_2ATP, 2.5 $MgCl_2$, 0.1 $CaCl_2$, pH 7.4. For the low chloride experiments, pipettes were either filled with an intracellular solution containing (in mM): 62.5 K_2SO_4, 10 KCl, 5 EGTA-KOH, 5 HEPES, 2.5 $MgCl_2$, 2.5 K_2ATP, 0.1 $CaCl_2$, 62.5 glucose pH 7.4 or with 125 potassium gluconate, 10 KCl, 5 EGTA-KOH, 5 HEPES, 2.5 K_2ATP, 2.5 $MgCl_2$, 0.1 $CaCl_2$, pH 7.4. Currents were recorded in the whole-cell voltage-clamp configuration at room temperature using an Axopatch 200B (Molecular devices, Palo Alto, CA), filtered at 1 kHz with a low pass Bessel filter, digitized at ≥20 kHz with a 12-bit acquisition board (Digidata 1322) and pClamp 8.2 (Molecular Devices) and stored on disk for offline analysis using OriginPro 7.1 (OriginLab, Northampton, MA). Results are presented as means ± S.D. Statistical analysis was completed in OriginPro 7.1. Analysis of Variance (ANOVA) tests were used to compare multiple means using a Tukey pairwise post-hoc comparison of individual means.

Vestibular Evoked Potentials

VsEPs were recorded from mice of either sex at 9 months of age from four genotypes with the investigator blind to the genotype. We used a standard noninvasive recording procedure recently described in Mock et al. (2011). Briefly, mice were anesthetized with ketamine (90 - 126 mg/kg) and xylazine (10 - 14 mg/kg) injected intraperitoneally and core body temperature was maintained at 37.0 ± 0.2°C using a homeothermic heating pad system (FHC, Inc.). Subcutaneous needle electrodes were placed just posterior to the lambdoidal suture (noninverting), behind the right pinna (inverting) and at the neck (ground). A noninvasive head clip was used to secure the head to a mechanical shaker for delivery of vestibular stimuli. Linear acceleration pulses (17 pulses/sec, 2 ms duration) were presented to the cranium in the naso-occipital axis. Stimulus amplitude ranged from +6 dB to – 18 dB re: 1.0 g/ms (where 1 g = 9.8 m/s^2) adjusted in 3 dB steps. Electroencephalographic activity was amplified (200,000X), filtered (300 to 3000 Hz, -6 dB amplitude points) and digitized (1024 points, 10 μs/pt). 256 primary responses were averaged and replicated for each VsEP waveform. The first positive (P1) and negative (N1) response peaks were scored for VsEPs since this initial response peak is generated by the peripheral eighth nerve. Peak latencies (measured in milliseconds, ms), peak-to-peak amplitude (measured in microvolts, μV) and thresholds (measured in dB re: 1.0 g/ms) were quantified and compared across genotypes.

Rotarod behavior

An initial cohort of 18 mice of either sex from control and *Hcn1*-deficient strains were used for behavioral testing according to standard protocols (Clabough and Zeitlin, 2006). The strain of the control mice was B6129SF2/J and the strain of the HCN1-deficient mice was B6;129-*Hcn1*^{tm2Kndl}/J (The Jackson Laboratory). Animals were tested between 1.5 months and 2 months of age on one of two testing days. Testing was done at approximately the same time of day, and all genotypes were tested on a given day in order to minimize environmental variability. A follow up study was completed using 50 mice of either sex from three separate strains: *Hcn1*-floxed mice, *Hcn1*-floxed mice positive for *Cre-recombinase*, and *Hcn1*$^{+/+}$ mice positive for *Cre-recombinase*. All behavioral data were acquired with the investigator blind to the genotype.

Behavioral data were collected from an Economex Accelerating Rotarod (Columbus Instruments) which allowed us to test up to four mice at one time. All mice were tested using the following rotarod protocol. Testing occurred in three phases: 1) Mice were placed on a stationary rotarod for up to 60 seconds or until falling, whichever occurred first. Latency to fall was recorded automatically via a pressure sensitive floor panel. If the mouse fell immediately after placement on the rod, no time was recorded and the mouse was immediately replaced on the rod. If the mouse fell again, a time of 1 second was recorded. This training paradigm was repeated two more times with no inter-trial interval. A second set of three training trials was repeated for each mouse approximately 15 minutes after completion of the first set. 2) In the second training phase mice were placed on the rotarod at a constant speed of 2 rotations/minute (RPM) for up to 60 seconds. Latency to fall was recorded. This training was repeated two more times with no inter-trial interval. Again, if a mouse fell before the timer could be started it was immediately replaced on the rod. If it fell again, a score of 1 second was recorded. 3) In the third phase the mice were tested for three trials on a rotarod accelerating at 0.1 rotations/minute^2 from an initial speed of 2 RPM with a 15 minute interval between each trial. Latency to fall was recorded. If a mouse fell before the acceleration was turned on, it was immediately replaced on the rod. After three trials on the accelerating rotarod, each mouse was tested in a final trial in a dark environment. Each mouse was placed on the rotarod in the light, and once all mice had been placed, the lights were extinguished and the acceleration initiated. Once all mice had fallen, the lights were turned back on and the latency to fall was recorded.

RESULTS

Expression of HCN Channels

To investigate the relative expression levels of *Hcn* transcripts in the mouse utricle, we used quantitative, RT-PCR (qPCR) and specific, validated primer sets as described previously for detection of *Hcn* gene expression in mouse cochlea (Horwitz et al., 2010). RNA was extracted from the sensory epithelia of ten utricles excised from B6129SF2/J postnatal day (P) 8 mice. We found *Hcn1* to be the most highly expressed subunit (Fig. 1*A*). The expression ratios for *Hcn1-4* were 499:145:1:30, respectively. This result was consistent with experiments performed in a trout saccule preparation which also demonstrated high levels of *Hcn1* mRNA (Cho et al., 2003).

Previous work indicated that I_h was acquired in mammalian vestibular hair cells during the middle of the first postnatal week (Rüsch et al., 1998). Using mRNA from utricle sensory epithelia harvested at four developmental ages, we compared expression of *Hcn1* and found that mRNA levels rose between P0 and P4 (Fig. 1*A*). No significant change was detected between P4 and P10, at which point murine vestibular hair cells are physiologically mature

(Rüsch et al., 1998). The change in *Hcn1* mRNA expression level is consistent with the temporal acquisition of I_h and may indicate a developmental role for the current.

In addition to hair cells, the tissue used for the qPCR analysis also contained nerve terminals and supporting cells. Because some of these cell types have also been shown to express I_h (Chabbert et al., 2001), we opted to localize HCN1 protein in the mouse utricle. We used an antibody specific to HCN1 (Horwitz et al., 2010) directed against the C-terminus of the protein. Figure 1*B* shows a projection of an image series taken through multiple focal planes. We found robust expression of HCN1 in the basolateral membranes of utricle hair cells harvested at P8 (Fig. 1*B*). Figure 1*C* shows a confocal image of a utricle sensory epithelium harvested from an *Hcn1*-deficient mouse. The gain and contrast levels have been boosted and revealed a lack of staining, confirming the specificity of the antibody.

To investigate whether HCN1 may also be expressed in afferent terminals of vestibular ganglion neurons we counterstained utricle epithelia with an antibody directed against neurofilament-200. Figure 1*D* shows a confocal image of a utricle sensory epithelium stained with both HCN1 and NF200. HCN1 staining is apparent in type II (thin arrows) and in type I hair cells (thick arrows) within the confines of calyx terminals which engulf type I cells. In some cases, HCN1 staining was colocalized with neurofilament-200, indicating that HCN1 may also be present in afferent terminals.

To quantify the percentage of hair cells that expressed HCN1, we counter stained utricle sensory epithelia tissue for Myosin 7a, a hair cell marker (Hasson et al., 1996). We counted the number of HCN1-positive cells and found that HCN1was expressed in 89% (n=113) of Myosin 7a-positive cells (Fig 1*E*). We also found evidence for HCN2 and HCN4 immunoreactivity in the utricle epithelium. However, the HCN2 and HCN4 staining was weaker and less prevalent than HCN1 and was not localized to hair cells (data not shown). Based on the mRNA expression patterns and immunolocalization, HCN1 seems to be the most prominent HCN subunit in mouse utricle hair cells.

Characterization of I_h in mouse vestibular hair cells

The basolateral membrane localization pattern suggested that HCN subunits may contribute as a voltage-gated conductance and may help shape graded receptor potentials in vestibular hair cells. To investigate the contribution of HCN subunits to hair cell function and to facilitate comparison with prior studies we began with a biophysical characterization of I_h. We used the whole-cell, tight-seal technique to record from type I and type II hair cells of the mouse utricle. From a holding potential of −64 mV, we delivered 2-second steps at voltages that ranged between −144 and −44 mV in 10 mV increments. In wild-type type II hair cells the protocol evoked slowly activating inward currents (Fig. 2*A*). In type I hair cells (Fig. 2*B*), the same protocol evoked large inward currents that subsequently deactivated consistent with $I_{K,L}$, as previously described (Rüsch and Eatock, 1996). Following deactivation of $I_{K,L}$, activation of I_h was apparent with kinetics and amplitudes similar to those of I_h in type II cells. We found robust expression of I_h in 89% of type II hair cells (n = 47), and in 78% of type I hair cells (n = 28). Qualitatively, the properties of I_h in mouse vestibular hair cells were similar to those of I_h in other hair cell preparations (Holt and Eatock, 1995; Rüsch et al., 1998; Sugihara and Furukawa, 1996; Brichta et al., 2002).

To generate I_h activation curves with minimal contamination, tail currents were measured at −74 mV, near the reversal potential for the potassium-selective inward rectifier, I_{K1}. The tail current was sampled at the moment of the step to −74 mV and plotted against prepulse potential. Conductance was calculated by dividing the I_h tail current by the difference (30 mV) between the step potential (−74 mV) and the experimentally determined reversal potential (−44 mV, as measured from type II hair cells in the presence of 500 μM $BaCl_2$

which blocked I_{K1}). Type II vestibular hair cells had a maximum conductance of 4.4 ± 2.6 nS, a half-activation voltage of −99 ± 6 mV and a slope factor of 8.5 ± 1.9 mV (n = 41; Fig. 2*C*). Under our experimental conditions, the conductance of I_h was slightly larger than previously reported in mouse vestibular hair cells (Rüsch et al., 1998), perhaps due to differences in the age of the cells or rundown of I_h. Because I_h can be modulated by a number of intracellular factors, the current can quickly run down upon break through to whole–cell mode. As such, the I_h data presented here were recorded immediately after breakthrough to the whole-cell configuration.

To investigate the chloride sensitivity, we recorded I_h from 14 hair cells (data not shown) using two alternate low chloride solutions (15 mM, see Materials and Methods), but found no difference in the amplitude, kinetics or activation range relative to I_h recorded with our standard pipette solution. Since I_h has also been reported to be sensitive to cAMP (Wainger et al., 2001), we generated activation curves from nine type II hair cells in the presence of 200 μL of membrane permeable 8-Br-cAMP. We found that the activation curve shifted 6.7 mV in the positive direction (Fig. 2*D*) with little effect on other biophysical properties. This shift was nearly identical to the shift measured for HCN1 expressed in heterologous cells (Wainger et al., 2001).

Type I hair cells had a maximum conductance of 4.2 ± 1.8 nS (n = 22) which was not significantly different from the conductance in type II hair cells. However, the half-activation voltage of I_h in type I vestibular hair cells was depolarized (−90 ± 5 mV; $p<0.001$) relative to type II cells. The slope factor of 6.8 ± 1.5 mV was also significantly ($p<0.001$) different than that measured in type II hair cells, indicating a difference in voltage dependence. Because type I hair cells express $I_{K,L}$ which is active at voltages that overlap with I_h activation we were reluctant to draw strong conclusions from these differences between I_h in type I and type II cells. However, since $I_{K,L}$ deactivates at potentials negative to −120 mV (Rüsch and Eatock, 1996; Holt et al., 2007), the maximum conductance values measured from tail currents after 2 second steps to −144 mV were accurate.

To characterize the activation kinetics of I_h, we fit currents from type II hair cells with double exponential functions and measured the time constants of activation. Currents were measured in the presence of 100 μM extracellular Ba^{2+} to block the fast inward rectifier, I_{K1}. We found that I_h activated rapidly at −144 mV and more slowly at −124 mV and −104 mV (Fig. 2*E*). Fast time constants of activation were 48 msec, 71 msec and 166 msec for currents measured at −144 mV, −124 mV and −104 mV, respectively (Fig. 2*F*). These time constants are consistent with those for HCN1 expressed in heterologous cells (Santoro et al., 1998; Santoro et al., 2000).

We examined the expression of I_h as a function of development and found little I_h at P0, followed by a dramatic rise over the first postnatal week (Figs. 3*A-D*). Beyond the first week I_h expression leveled off and we saw no further increase through adulthood. This pattern was consistent with a previous report that documented the development of I_h in mouse utricle hair cells (Rüsch et al., 1998). We also examined the position and slope of the activation curve as well as the kinetics of activation. In type II cells, there was a slight but statistically insignificant shift in the half-activation voltage from −104 mV at P0 to −96 mV at P10. We also observed little change in other biophysical properties of I_h as function of development (Figs. 3*F-G*). Since whole-cell capacitance remained constant through postnatal development (Fig. 3*H*) and most biophysical properties were unchanged, we conclude that the increase in conductance during development was due to an increase in the density of a relatively uniform population of channels.

Inhibition of I_h in *Hcn*-deficient hair cells

To investigate the ion channels that carry I_h, we applied HCN antagonists, ZD7288 and Cilobradine. Application of 100 μM ZD7288 or 10 μM Cilobradine completely abolished I_h (Fig. 4*B* & 4*C*) compared to control (Fig. 4*A*). At these concentrations there was little effect on mechanotransduction currents (Horwitz et al., 2010) and voltage-dependent currents, including the fast K^+-selective inward rectifier, I_{K1}. I_{K1} is apparent as the inward currents that remained in Figure 4*B* & 4*C*. Thus, at the concentration used here both drugs were selective for I_h, but could not distinguish amongst the different members of the HCN family. Further evidence implicating the *Hcn* gene family was derived from adenoviral transfection of a mutant form of *Hcn2* (Horwitz et al., 2010). Briefly, the GYG pore sequence of HCN2 was replaced with an AYA mutation, which yielded a dominant-negative subunit. The construct was packaged into adenoviral vectors which also contained the coding sequence for GFP as a transfection marker. Previously, the AYA mutant HCN2 was shown to coassemble with all other HCN subunits and suppress their function in a dominant-negative manner (Er et al., 2003). Utricles were excised at P1-P2, placed in culture and exposed to Ad-*Hcn2*-AYA for 4-24 hours. Approximately 6-7 days after transfection, at or near the equivalent of P8, we recorded from transfected, GFP-positive cells and untransfected, GFP-negative control cells. We were unable to evoke I_h in 12 of 16 utricle hair cells that expressed GFP. An image of a GFP-positive cell with recording pipette is shown in Fig. 4*F*. In the 4 of 16 cells with residual I_h (Fig. 4*D*), the amplitude of the currents was significantly reduced relative to wild-type cells. Neighboring non-transfected (GFP-negative) cells had I_h with amplitudes similar to those recorded from hair cells acutely excised from wild-type mice at P8 (Fig. 4*E*). The data from 94 type II cells are summarized in Fig. 4*G*. These data confirm that the hyperpolarization-activated currents in hair cells are carried by HCN subunits.

However, since neither the pharmacologic antagonists nor the AYA form of HCN2 suggest which HCN subunits contribute to the hair cell I_h, we recorded from hair cells excised from mice with targeted deletions of *Hcn1* and/or *Hcn2*. Mice deficient for *Hcn1* were obtained from Nolan et al. (2003) and mice deficient in *Hcn2* were obtained from Ludwig et al. (2003). Both type I (n = 19) and type II (n = 21) vestibular hair cells that were deficient in *Hcn1* lacked I_h entirely (Fig. 5*B*), whereas *Hcn2*-deficient hair cells had I_h with amplitudes of 4.2 ± 2.7 nS (n = 8; Fig. 5*C*), similar to wild-type (Fig. 5*A*). As described earlier, we generated activation curves for I_h measured from *Hcn2*-deficient hair cells and analyzed the voltage dependence. We found a half activation of −95.2 ± 5.6 mV with a slope factor of 8.3 ± 1.4 mV (n = 7). The kinetics of I_h activation at −124 mV were measured in *Hcn2*-deficient type II cells (τ_{fast} = 85.4 ± 15.4; n = 6). None of these values were significantly different from those measured in wild-type type II hair cells, suggesting that HCN2 does not contribute to I_h in mouse vestibular hair cells.

As expected, based on the absence of *Hcn1* (Fig. 5*B*), hair cells deficient for both *Hcn1* and *Hcn2* also lacked I_h (Fig. 5*D*). The mean maximal conductances measured from tail currents from 119 type II hair cells of the genotypes indicated are summarized in Figure 5*F*. Based on the molecular and immunohistochemical data, biophysical properties, lack of I_h in *Hcn1*-deficient hair cells, normal I_h in *Hcn2*-deficient cells, minimal expression of *Hcn3* in vestibular end organs and the lack of hair cell localization for HCN2 and HCN4, we conclude that HCN1 is necessary for I_h in mouse vestibular hair cells and is likely the primary HCN subunit. However, since mice deficient in *Hcn3* or *Hcn4* are not viable, we cannot rule out minor contributions from *Hcn3* or *Hcn4* that were below our immunolocalization, qPCR, and electrophysiological detection limits.

HCN1 channels expressed in rod photoreceptors have an estimated the single channel conductance of 663 – 766 fS (Barrow and Wu, 2009). If we assume that the maximal

conductance we measured in type II cells (4.4 nS) represents an open probability of 1 and use the Barrow and Wu single channel conductance estimate we calculate that type II vestibular hair cells have 5,744 – 6,636 HCN1 channels/cell, which corresponds to 22,976 – 26,544 protein monomers/cell. If the maximal open probability is less than one, these values would be larger.

Functional contributions of HCN1 in vestibular hair cells

Based on the preceding data we conclude that I_h in vestibular hair cells is composed primarily of HCN1 subunits. As such, we can use the tools described in the previous sections HCN antagonists, dominant-negative *Hcn2* mutations and genetic deletion of *Hcn1* to identify the functional contributions of HCN1 to sensory signaling in hair cells. I_h is active at the hair cell resting potential and is further activated by hyperpolarization. Thus, we hypothesized that I_h may contribute to resting potential; depolarization of the membrane in response to hyperpolarizing current steps; and enhanced excitability for small depolarizing stimuli, particularly following hyperpolarization. To test these hypotheses we injected small current steps and recorded the voltage response in current-clamp mode. At rest, hair cells have 10-20% of their transduction conductance active (Hudspeth, 1989). Therefore, we designed hyperpolarizing current steps from rest with physiologically relevant amplitudes of 50 pA, roughly equivalent to the maximal current decline that might result from negative hair bundle deflections and closure of transduction channels open at rest. Small hyperpolarizing currents may also result from efferent feedback to both type I and type II hair cells (Holt et al., 2006). The small current step size also ensured that the amplitude of the hyperpolarization remained within a physiological range, positive to ~ −90 mV, the most negative equilibrium potential for potassium, based on physiologically relevant potassium concentrations.

Following the onset of the current step, there was a rapid 20-30 mV hyperpolarization which was invariably followed by a depolarizing sag of 5 to 10 mV (Fig. 6*A*, small arrow). The sag presumably reflected activation of HCN1, which at −90 mV activated further and allowed small inward currents sufficient to depolarize the membrane in the direction of the resting potential. At the termination of the current step there was often a significant rebound which frequently overshot the resting potential by 15-20 mV (Fig. 6*A*, big arrow). We suspected that the sag, the rebound amplitude and the rebound latency were affected by current that flowed through HCN1 channels open during the hyperpolarizing step. To confirm these suspicions we applied HCN antagonists and subsequently measured a significant reduction in both the depolarizing sag during the current step and in the rebound at the end of the current step. The traces shown in Figure 6*A* and 6*B* are from the same cell before and after application of 100 μM ZD7288. Figure 6*C* and 6*D* are from a different cell before and after application of 10 μM Cilobradine. Both antagonists had similar effects on the voltage responses of vestibular hair cells to current injections.

To confirm that both the sag and the rebound were dependent upon I_h activation we designed a current-clamp protocol in which we hyperpolarized the membrane for increasing durations. Twenty msec after the onset of the current step there was little evidence of a sag or rebound at the end of the step (Fig. 6*E*). However, 100 msec later the sag and the rebound were apparent. Their amplitudes increased with longer steps. Since the temporal appearance of both the sag and the rebound paralleled the activation of I_h we suggest that inward current through HCN1 channels was sufficient to depolarize the membrane and produce both the sag and rebound potentials. Indeed, pharmacologic inhibition of I_h with ZD7288 abolished the sag and rebound regardless of the duration of the current step (Fig. 6*F*).

We also noted a similar reduction in the sag and a diminished rebound in hair cells of *Hcn1*-deficient mice (Fig. 7*A*) and in cells transfected with the HCN2-AYA construct (Fig. 7*C*).

Consistent with the conclusion that HCN1 is the most significant component of the hair cell I_h, mice that lacked *Hcn2* had sags and rebounds that were indistinguishable from wild-type cells (Fig. 7*C*). The presence or absence of I_h had little effect on the hair cell resting potential. We noticed a slight, but statistically insignificant hyperpolarization of the resting potential following application of HCN antagonists. Similarly, there were slight but insignificant differences in resting potential in HCN2-AYA transfected cells, *Hcn1*- and *Hcn2*-deficient cells (Fig. 7*D*).

Figures 7*E* and 7*F* summarize the sag potentials and rebound potentials in various conditions. The sag potential was measured as the difference between the peak hyperpolarization and the steady-state potential near the end of the step. The rebound potential was taken as the difference between the resting potential and the peak depolarization after the termination of the step. We pooled the data using the two different HCN antagonists since both were effective I_h blockers and both had no effect on other conductances at the concentrations tested. The data before and after drug application provide the most relevant comparison for indicating the contribution of I_h to the hair cell membrane response. Since the data are taken from the same cell, the amplitudes of all other hair cell conductances are identical in the two conditions. The comparison between wild-type, HCN2 AYA transfected cells, *Hcn1*- and *Hcn2*-deficient cells not only involves presence or absence of I_h, but are confounded by cell-to-cell variability in the amplitude of other voltage-gated conductances, cell capacitance and the like. As such, we feel the marked difference in the sag potential and in the rebound potential before and after application of HCN antagonists is the best indication of HCN1's contribution to the hair cell membrane response. Nonetheless, we note similar but smaller amplitude effects in HCN2-AYA transfected cells and in *Hcn1*-deficient cells but not in *Hcn2*-deficient cells.

To further consider the contributions of HCN1 to the hair cell membrane potential we examined the latency of the rebound following hyperpolarizing current steps. Figure 7*G* shows an expanded view of the membrane response recorded from a wild-type cell (thin line) and an *Hcn1*-deficient cell (thick line). We measured latency as the time from the end of the hyperpolarizing step to the peak of the rebound (arrowheads) in 70 different cells (Fig. 7*H*). Regardless of experimental manipulation – pharmacologic blockade, dominant-negative inhibition or genetic deletion – cells that lacked HCN1 activity had longer mean latencies (line) than cells with functional HCN1, whereas cells deficient in *Hcn2* had latencies that were similar to wild-type. Furthermore, as is apparent from the scatter (Fig. 7*H*), the variability in latency was much greater in cells that lacked *Hcn1*. As such, we conclude that activation of HCN1 contributes to the amplitude and speed of the rebound potential and helps synchronize hair cell responses, particularly for small stimuli.

Behavioral tests of balance function in *Hcn*-deficient mice

To assay for balance function we performed several rotarod tests. In order to test gross balance function and acclimate the mice to the behavioral task, wild-type and $Hcn1^{-/-}$ mice were placed on a stationary rotarod and the total time spent on the rod before falling was recorded up to a maximum of 60 seconds. Each naïve mouse was trained in this way over two sets of three trials. The data are summarized in Figure 8*A* for five wild-type mice and 13 *Hcn1*-deficient mice. *Hcn1*-deficient mice performed poorly relative to wild-type mice, often falling immediately after being placed on the apparatus, but showed marked improvement with each subsequent trial until most could stay on the full 60 seconds.

In the next assay, the rotarod accelerated at 0.1 rotations/minute^2 from an initial speed of 2 rotations/minute. Each mouse that demonstrated an ability to balance on the stationary rotarod for 60 seconds was tested on the accelerating rotarod three times. Again, the *Hcn1*-

deficient mice performed significantly worse, typically falling off the device within the first minute (Fig. 8*B*).

Proper balance function utilizes sensory input from three sensory systems: the vestibular system, the visual system and proprioception. Mice and humans can learn to compensate for a loss of input from any one of the three, however, loss of two of the three systems presents a greater challenge. To challenge the balance function of the mice we performed the same accelerating rotarod test in a dark environment immediately following the previous three trails. Wild-type mice had little difficulty with the loss of visual input and remained on the rotarod for about the same time: ~2.5 minutes whether the lights were on or off. However, the performance of the *Hcn1*-deficient mice regressed in the dark environment, with the mice falling off the accelerating rotarod in less than a minute, indicating significant balance problems.

Conditional deletion of *Hcn1*

Since *Hcn1* expression has been identified in the cardiovascular system and throughout the central and peripheral nervous system (DiFrancesco, 2006; Wahl-Schott and Biel, 2009) and has been shown to be important for motor learning (Nolan et al., 2003), we wondered whether the rotarod deficit (Fig. 8) was the result of *Hcn1* deletion in tissues other than the vestibular periphery. To address this possibility we used conditional deletion of *Hcn1* in the inner ear. We began by examining hair cells of mice that carried the *Hcn1* gene with lox P sites that flanked the pore loop and the S4 region (Nolan et al., 2003). To restrict deletion of *Hcn1* to individual hair cells, utricles were excised at P0-P2 from *Hcn1*-floxed mice and were transfected with an adenovirus that expressed Cre-recombinase and GFP as a transfection marker. Control hair cells from *Hcn1*-floxed mice (Fig. 9*A*) had I_h indistinguishable from wild-type, indicating that the floxed allele did not alter *Hcn1* expression. GFP-positive hair cells transfected with Ad-Cre had no I_h, consistent with the data from *Hcn1*-deficient mice (Fig. 9*B*). As a control for adenoviral expression of Cre recombinase, we also recorded from wild-type hair cells transfected with Ad-Cre-GFP and found normal I_h amplitudes (Fig. 9*C*). Next we crossed the *Hcn1*-floxed mice with mice that expressed Cre-recombinase driven by the *Foxg1* promoter which is active in inner ear tissue beginning at embryonic day 10.5 (Pauley et al., 2006), well before the appearance of I_h (Géléoc et al., 2004). Offspring homozygous for the *Hcn1*-floxed allele and heterozygous for *Foxg1-Cre* displayed no residual I_h (Fig. 9*D*) which resembled the result from the global *Hcn1*-deficient tissue. The data from 31 type II hair cells are summarized in Figure 9*E*.

To investigate whether the behavioral deficit displayed in Figure 8 resulted from the loss of I_h within the inner ear or elsewhere we used the same rotarod paradigm and tested mice from three genotypes: 1) homozygous *Hcn1*-floxed, 2) $Hcn1^{+/+}$; heterozygous *Foxg1-Cre* and 3) homozygous *Hcn1*-floxed; heterozygous *Foxg1-Cre*. Figure 9*F* shows the data from six stationary training trials for which 50 mice were tested. Mice with inner ear deletion of *Hcn1* (white bars) performed poorly compared to the *Hcn1*-floxed littermates that lacked *Cre-recombinase* (gray bars). To control for behavioral effects of the *Foxg1-Cre* allele, we tested six $Hcn1^{+/+}$ mice heterozygous for *Foxg1-Cre* (striped bars) and found no significant difference in any of the six trials relative to the *Hcn1*-floxed mice that lacked Cre expression.

The *Hcn1*-floxed mice heterozygous for *Foxg1-Cre* were tested on the accelerating rotarod paradigm and performed poorly in two of the four testing trials compared to *Hcn1*-floxed mice that lacked *Cre* (Fig. 9*G*). We observed no significant difference between the *Hcn1*-floxed mice (gray bars) and the *Foxg1-Cre* heterozygous mice (striped bars) suggesting that they both had normal balance function. However, while the *Hcn1*-floxed mice that lacked *Cre-recombinase* performed steadily from trial three to the dark trial (trial four), the mice

with inner ear deletion of *Hcn1* performed significantly worse in the dark. As such, we suggest that in the absence of visual input the mice are forced to rely on proprioception and vestibular function, the latter of which appears to be compromised in the mice with inner ear of deletion of *Hcn1*.

To investigate the link between the deficit observed in hair cells and the behavioral deficit in *Hcn1*-deficient mice we recorded vestibular evoked potentials (VsEPs). VsEPs provide a noninvasive measure of the summed activity in the vestibulocochlear nerve (the eighth cranial nerve) in response to head movements. We tested VsEPs in 28 mice: 14 *Hcn1*-floxed mice, 10 *Hcn1*-floxed; *Foxg1-Cre* mice and 4 conventional *HCN1*-deficent mice. We saw no differences in response threshold and no differences in latency to the first peak, suggesting vestibular sensitivity and the speed of signal transmission were unaltered in *Hcn1*-deficient mice. However, we measured a significant difference in the amplitude of the first peak particularly for low stimulus levels, 3 dB and 6 dB, between the conventional *Hcn1*-deficent mice and the *Hcn1*-floxed mice (Fig. 9*H*) and between *Hcn1*-floxed mice the *Hcn1*-floxed; *Foxg1-Cre* mice (Fig. 9I). Since the amplitude of the first peak of the VsEP response reflects the degree of synchronous firing in the 8th nerve we suggest that the reduced VsEP amplitude recorded from the *Hcn1*-deficient mice may result from a loss of synchronous activity in the 8th nerve which in turn may be a direct result of the large scatter in rebound latency that we documented in *Hcn1*-deficent hair cells (Fig. 7*H*).

DISCUSSION

I_h in hair cells is carried by HCN1 channels

Although I_h has been characterized in vestibular hair cells of a number of species including frogs (Holt and Eatock, 1995), goldfish (Sugihara and Furukawa, 1996), turtles (Brichta et al., 2002), pigeons (Masetto and Correia, 1997) and mice (Rüsch et al., 1998), the molecular correlates of the hair cell I_h have not been identified. Cho et al. (2003) examined *Hcn* gene expression in vestibular organs of the trout and identified *Hcn 1, 2* and *4*. Based on their finding that *Hcn1* was the most highly expressed subunit, they hypothesized that HCN1 may be the principle channel subunit that carries I_h in hair cells (Cho et al., 2003). Given that we found *Hcn1* mRNA expression levels to be ~500-fold higher than *Hcn3*, our qPCR data were consistent with their hypothesis. Our immunolocalization data also supported a prominent role for HCN1 in mammalian hair cells as HCN1 protein was localized to the basolateral membranes of mouse vestibular hair cells. The strongest data supporting the hypothesis that the hair cell I_h is carried by HCN1 channels are derived from our electrophysiological assays. The complete loss of I_h in *Hcn1* knockout mice, together with normal I_h in *Hcn2* knockout mice suggests that HCN1 is both necessary and sufficient to form the channels that carry I_h in vestibular hair cells.

Function of HCN1 in vestibular hair cells

Based on the biophysical properties of I_h we predicted that HCN1 makes several functional contributions to sensory signaling in vestibular hair cells. Because HCN1 channels have a reversal potential of ~ −40 mV, and are partially activated at rest, we predicted that HCN1 would tend to depolarize the hair cell resting potential. This was not the case *in vitro*. We noticed small, but statistically insignificant changes in resting potential in cells that lacked I_h. We suspect that small alterations in open probability of other ion channels active at rest, such as sodium (Wooltorton et al., 2007), calcium (Bao et al., 2003) or transduction channels (Farris et al., 2006), may have compensated for the loss of I_h.

We also predicted that activation of I_h might tend to counteract small hyperpolarizations of the hair cell membrane potential. In hair cells, small hyperpolarizations can result from

deactivation of transduction channels open at rest or efferent synaptic transmission which releases acetylcholine to activate calcium-permeable nicotinic receptors and subsequently calcium-dependent potassium channels (Holt et al., 2006). For either transduction deactivation or efferent activation, the most extreme hyperpolarizations are not expected to extend negative to the potassium equilibrium potential, ~ −90 mV.

We found that physiologically-relevant hyperpolarizing currents evoked a depolarizing sag in the membrane response with a time course that paralleled the activation of I_h. Regardless of the experimental manipulation, inhibition of I_h nearly abolished the sag. In addition to its contribution to the sag potential, activation of I_h enhanced the depolarizing rebound at the end of the hyperpolarizing step. We noticed a substantial rebound that was significantly reduced by inhibition of I_h. The rebounds routinely extended 10-20 mV positive to the activation threshold for calcium channels ~ −60 mV (Bao et al., 2003). We suspect that I_h-enhanced rebounds may evoke substantially more calcium channel activation, calcium influx, synaptic vesicle fusion and neurotransmitter release. If so, we hypothesize that HCN1 activity in vestibular hair cells may contribute to an off response (Mitra and Miller, 2007) in afferent neurons at the cessation of vestibular stimulation.

We also noticed that hair cells that expressed functional I_h had shorter rebound latencies and furthermore that the latencies were more tightly synchronized among hair cells. Cells that lacked functional I_h, regardless of experimental manipulation, had greater scatter in their latency distribution. As such, we suggest that another important role of HCN1 may be to speed and synchronize hair cell activity, particularly for small stimuli.

Contribution of HCN1 to vestibular function

HCN1 may contribute to synchronous firing of vestibular afferent fibers in response to small stimuli. The first peak in vestibular evoked potentials records the summed vestibular afferent activity in the 8th cranial nerve in response to head movements. We saw no difference in threshold or latency in any of the mouse genotypes we examined indicating that vestibular sensitivity and the speed of action potential propagation were unaltered. However, for small stimuli there were significant reductions in the amplitude of the first VsEP peak in mice that lacked HCN1, indicating that there was greater temporal scatter in 8th nerve activity. We suggest that the reduced vestibular nerve synchrony was a direct result of the loss of HCN1 in vestibular hair cells since those cells had reduced synchrony in rebound latency. Synchronous activity of vestibular afferents may enhance the signal to noisy ratio and vestibular sensitivity, particularly for small stimuli. We cannot rule out that loss of HCN1 activity in vestibular neurons themselves may have also contributed to the deficit.

Another consequence of HCN1 activity in hair cells may be modulation of spontaneous vestibular afferent activity (Trapani and Nicolson, 2011). Vestibular afferent fibers display a wide range of firing patterns and are spontaneously active (Eatock et al., 2008). Spontaneous afferent activity is likely the result of release of transmitter from hair cells, since vestibular neurons in denervated preparations without hair cell end organs lack spontaneous activity (Risner and Holt, 2006; Kalluri et al., 2010; Trapani and Nicholson, 2011). As such, we suspect that HCN1 activity in hair cells may contribute to spontaneous firing in vestibular afferents. Since the activation / deactivation kinetics of HCN1 channels are too slow to follow rapid changes in the hair cell membrane potential, we propose that low frequency or tonic HCN1 activation would enhance depolarization of hair cell membrane potentials into the range where calcium channels are active, which may in turn affect neurotransmitter release and vestibular afferent firing patterns.

Although we found no significant difference in the hair cell resting potential in *Hcn1*-deficient mice *in vitro*, a number of intracellular factors have been identified that can

modulate HCN1 activity including cAMP, PIP_2, pH, phosphorylation by p38-MAP kinase, and several binding partners such as MiRP1 and TRIP8b (Wahl-Schott and Biel, 2009). Many of these factors affect the voltage dependence and activation range of I_h. We found that application of the non-hydrolyzable cAMP analog, 8-Br-cAMP shifted the voltage-dependence of the hair cell I_h by +7 mV. Factors that shift the I_h activation curve in the positive direction would result in greater activation at rest and would tend to enhance the contributions of I_h to the hair cell membrane potential whereas factors that shift the activation range in the negative direction would tend to diminish the impact of I_h. As such, modulation of HCN1 activity *in vivo* may allow hair cells the ability to regulate activity at rest and their response to small stimuli.

Contribution of HCN1 to balance function

In addition to the HCN1 contribution to hair cell function and vestibular afferent activity we found HCN1 important in behavioral assays of balance function. Mice that lacked *Hcn1* globally, as well as animals with *Hcn1* deletion in the inner ear, had balance deficits when challenged with rotarod tasks. Because proper balance function utilizes sensory input from vestibular, visual and proprioceptive systems and requires proper cerebellar function and motor output, the rotarod deficit in mice with global deletion of *Hcn1* indicates that HCN1 is a necessary component of the balance pathway and may well perform critical functions at multiple loci along the pathway. Nolan et al. (2003) found that mice globally deficient in *Hcn1* suffered learning and memory deficits in rotarod tasks and concluded that motor learning and cerebellar function were compromised but that basic motor function remained intact. Since the Nolan et al. study (2003) did not examine vestibular function, we opted to use a rotarod protocol designed to highlight subtle vestibular dysfunction. During a series of trials on a single day we observed significant baseline balance deficits in naïve *Hcn1*-deficient mice relative to wild-type mice. These data suggest that in addition to a role in cerebellar motor learning, HCN1 may also play a role in normal sensory function along the balance pathway.

To identify which sensory system requires HCN1 expression for normal balance function, we crossed *Hcn1*-floxed mice with mice that expressed Cre-recombinase under control of the *Foxg1* promoter. *Foxg1* promoter activity along the balance pathway is restricted to the inner ear including hair cells and vestibular neurons (Pauley et al., 2006) and is not active elsewhere along the pathway. We found that mice that lacked HCN1 expression in the inner ear suffered similar hair cell, VsEP and rotarod deficits to the mice with global *Hcn1* deletion. On the other hand, *Hcn1*-floxed mice that lacked Cre expression and mice that expressed Cre in the absence of *Hcn1*-floxed alleles had normal responses in hair cell, VsEP and rotarod assays. Importantly, we also found that when the balance function of mice with inner ear deletion of *Hcn1* was further challenged on the rotarod task in the dark, their performance was more severely compromised. In this experimental paradigm, the absence of visual compensation further illuminates the contribution of vestibular HCN1 expression to normal balance function. Whether HCN1 contributes to vestibular ganglion neuron function remains to be determined.

Lastly, we note that Ivabradine, a drug chemically similar to Cilobradine approved for clinical use in Europe to target HCN function and slow heart rate, has side effects that include dizziness and severe vertigo (Zhang et al., 2008). Since I_h has been identified in type II hair cells harvested from human vestibular organs (Oghalai et al., 1998) and because Ivabradine does not cross the blood-brain barrier, we speculate that these side effects may arise from its action on HCN targets within the vestibular periphery.

Acknowledgments

We thank members of the Holt/Géléoc lab for helpful discussions, Laura Digilio for help with animals, the Zeitlin lab for use of equipment and Andreas Ludwig for sharing *Hcn2* knockout mice. This work was supported by the NIH/NIDCD grants DC05439 (J.R.H.) and DC006443 (S.M.J.) and the Neurobiology and Development Training Program 5T32HD007323-24.

REFERENCES

Bader CR, Macleish PR, Schwartz EA. A voltage-clamp study of the light response in solitary rods of the tiger salamander. J Physiol. 1979; 296:1–26. [PubMed: 529060]

Bao H, Wong WH, Goldberg JM, Eatock RA. Voltage-gated calcium channel currents in type I and type II hair cells isolated from the rat crista. J Neurophysiol. 2003; 90:155–164. [PubMed: 12843307]

Barrow AJ, Wu SM. Low-conductance HCN1 ion channels augment the frequency response of rod and cone photoreceptors. J Neurosci. 2009; 29:5841–5853. [PubMed: 19420251]

Biel M, Wahl-Schott C, Michalakis S, Zong X. Hyperpolarization-activated cation channels: from genes to function. Physiol Rev. 2009; 89:847–885. [PubMed: 19584315]

Brichta AM, Aubert A, Eatock RA, Goldberg JM. Regional analysis of whole cell currents from hair cells of the turtle posterior crista. J Neurophysiol. 2002; 88:3259–78. [PubMed: 12466445]

Brown HF, DiFrancesco D, Noble SJ. How does adrenaline accelerate the heart? Nature. 1979; 280:235–236. [PubMed: 450140]

Cangiano L, Gargini C, Della Santina L, Demontis GC, Cervetto L. High-pass filtering of input signals by the Ih current in a non-spiking neuron, the retinal rod bipolar cell. PLoS One. 2007; 2:e1327. [PubMed: 18091997]

Chabbert C, Chambard JM, Valmier J, Sans A, Desmadryl G. Hyperpolarization-activated (Ih) current in mouse vestibular primary neurons. Neuroreport. 2001; 12:2701–2704. [PubMed: 11522951]

Cho WJ, Drescher MJ, Hatfield JS, Bessert DA, Skoff RP, Drescher DG. Hyperpolarization-activated, cyclic AMP-gated, HCN1-like cation channel: the primary, full-length HCN isoform expressed in a saccular hair-cell layer. Neurosci. 2003; 118:525–534.

Clabough EB, Zeitlin SO. Deletion of the triplet repeat encoding polyglutamine within the mouse Huntington's disease gene results in subtle behavioral/motor phenotypes in vivo and elevated levels of ATP with cellular senescence in vitro. Hum Mol Genet. 2006; 15:607–623. [PubMed: 16403806]

DiFrancesco D. A study of the ionic nature of the pace-maker current in calf Purkinje fibres. J Physiol. 1981; 314:377–393. [PubMed: 6273534]

DiFrancesco D. Serious workings of the funny current. Prog Biophys Mol Biol. 2006; 90:13–25. [PubMed: 15975637]

Eatock RA, Xue J, Kalluri R. Ion channels in mammalian vestibular afferents may set regularity of firing. J Exp Biol. 2008; 211:1764–1774. [PubMed: 18490392]

Er F, Larbig R, Ludwig A, Biel M, Hofmann F, Beuckelmann DJ, Hoppe UC. Dominant-negative suppression of HCN channels markedly reduces the native pacemaker current I(f) and undermines spontaneous beating of neonatal cardiomyocytes. Circulation. 2003; 107:485–489. [PubMed: 12551875]

Fain GL, Quandt FN, Bastian BL, Gerschenfeld HM. Contribution of a caesium-sensitive conductance increase to the rod photoresponse. Nature. 1978; 272:466–469. [PubMed: 416359]

Farris HE, Wells GB, Ricci AJ. Steady-state adaptation of mechanotransduction modulates the resting potential of auditory hair cells, providing an assay for endolymph [Ca2+]. J Neurosci. 2006; 26:12526–12536. [PubMed: 17135414]

Géléoc GS, Risner JR, Holt JR. Developmental acquisition of voltage-dependent conductances and sensory signaling in hair cells of the embryonic mouse inner ear. J Neurosci. 2004; 24:11148–11159. [PubMed: 15590931]

Halliwell JV, Adams PR. Voltage-clamp analysis of muscarinic excitation in hippocampal neurons. Brain Res. 1982; 250:71–92. [PubMed: 6128061]

Hebert JM, McConnell SK. Targeting of cre to the Foxg1 (BF-1) locus mediates loxP recombination in the telencephalon and other developing head structures. Dev Biol. 2000; 222:296–306. [PubMed: 10837119]

Holt JR, Eatock RA. Inwardly rectifying currents of saccular hair cells from the leopard frog. J Neurophysiol. 1995; 73:1484–1502. [PubMed: 7543944]

Holt JR, Corey DP, Eatock RA. Mechanoelectrical transduction and adaptation in hair cells of the mouse utricle, a low-frequency vestibular organ. J Neurosci. 1997; 17:8739–8748. [PubMed: 9348343]

Holt JC, Lysakowski A, Goldberg JM. Mechanisms of efferent-mediated responses in the turtle posterior crista. J Neurosci. 2006; 26:13180–13193. [PubMed: 17182768]

Holt JR, Stauffer EA, Abraham D, Geleoc GS. Dominant-negative inhibition of M-like potassium conductances in hair cells of the mouse inner ear. J Neurosci. 2007; 27:8940–8951. [PubMed: 17699675]

Horwitz GC, Lelli A, Geleoc GS, Holt JR. HCN channels are not required for mechanotransduction in sensory hair cells of the mouse inner ear. PLoS One. 5:e8627. [PubMed: 20062532]

Hudspeth AJ. Mechanoelectrical transduction by hair cells of the bullfrog's sacculus. Prog Brain Res. 1989; 80:129–135. discussion 127-128. [PubMed: 2699361]

Kalluri R, Xue J, Eatock RA. Ion channels set spike timing regularity of mammalian vestibular afferent neurons. J Neurophysiol. 2010; 104:2034–51. [PubMed: 20660422]

Ludwig A, Zong X, Jeglitsch M, Hofmann F, Biel M. A family of hyperpolarization-activated mammalian cation channels. Nature. 1998; 393:587–591. [PubMed: 9634236]

Ludwig A, Budde T, Stieber J, Moosmang S, Wahl C, Holthoff K, Langebartels A, Wotjak C, Munsch T, Zong X, Feil S, Feil R, Lancel M, Chien KR, Konnerth A, Pape HC, Biel M, Hofmann F. Absence epilepsy and sinus dysrhythmia in mice lacking the pacemaker channel HCN2. EMBO J. 2003; 22:216–224. [PubMed: 12514127]

Masetto S, Correia MJ. Electrophysiological properties of vestibular sensory and supporting cells in the labyrinth slice before and during regeneration. J Neurophysiol. 1997; 78:1913–1927. [PubMed: 9325360]

Mitra P, Miller RF. Mechanism underlying rebound excitation in retinal ganglion cells. Visual Neurosci. 2007; 24:709–731.

Mo ZL, Davis RL. Heterogeneous voltage dependence of inward rectifier currents in spiral ganglion neurons. J Neurophysiol. 1997; 78:3019–3027. [PubMed: 9405521]

Mock B, Jones TA, Jones SM. Gravity receptor aging in the CBA/CaJ strain: A comparison to auditory aging. J Assoc Res Otolaryngol. 2011; 12:173–83. [PubMed: 21052761]

Much B, Wahl-Schott C, Zong X, Schneider A, Baumann L, Moosmang S, Ludwig A, Biel M. Role of subunit heteromerization and N-linked glycosylation in the formation of functional hyperpolarization-activated cyclic nucleotide-gated channels. J Biol Chem. 2003; 278:43781–43786. [PubMed: 12928435]

Nolan MF, Malleret G, Lee KH, Gibbs E, Dudman JT, Santoro B, Yin D, Thompson RF, Siegelbaum SA, Kandel ER, Morozov A. The hyperpolarization-activated HCN1 channel is important for motor learning and neuronal integration by cerebellar Purkinje cells. Cell. 2003; 115:551–564. [PubMed: 14651847]

Noma A, Irisawa H. A time- and voltage-dependent potassium current in the rabbit sinoatrial node cell. Pflugers Arch. 1976; 366:251–258. [PubMed: 1033527]

Oghalai JS, Holt JR, Nakagawa T, Jung TM, Coker NJ, Jenkins HA, Eatock RA, Brownell WE. Ionic currents and electromotility in inner ear hair cells from humans. J Neurophysiol. 1998; 79:2235–2239. [PubMed: 9535985]

Pauley S, Lai E, Fritzsch B. Foxg1 is required for morphogenesis and histogenesis of the mammalian inner ear. Dev Dyn. 2006; 235:2470–2482. [PubMed: 16691564]

Risner JR, Holt JR. Heterogeneous potassium conductances contribute to the diverse firing properties of postnatal mouse vestibular ganglion neurons. J Neurophysiol. 2006; 96:2364–2376. [PubMed: 16855108]

Rusch A, Eatock RA. A delayed rectifier conductance in type I hair cells of the mouse utricle. J Neurophysiol. 1996; 76:995–1004. [PubMed: 8871214]

Rusch A, Lysakowski A, Eatock RA. Postnatal development of type I and type II hair cells in the mouse utricle: acquisition of voltage-gated conductances and differentiated morphology. J Neurosci. 1998; 18:7487–7501. [PubMed: 9736667]

Santoro B, Liu DT, Yao H, Bartsch D, Kandel ER, Siegelbaum SA, Tibbs GR. Identification of a gene encoding a hyperpolarization-activated pacemaker channel of brain. Cell. 1998; 93:717–729. [PubMed: 9630217]

Santoro B, Tibbs GR. The HCN gene family: molecular basis of the hyperpolarization-activated pacemaker channels. Ann N Y Acad Sci. 1999; 868:741–764. [PubMed: 10414361]

Santoro B, Chen S, Luthi A, Pavlidis P, Shumyatsky GP, Tibbs GR, Siegelbaum SA. Molecular and functional heterogeneity of hyperpolarization-activated pacemaker channels in the mouse CNS. J Neurosci. 2000; 20:5264–5275. [PubMed: 10884310]

Sugihara I, Furukawa T. Inwardly rectifying currents in hair cells and supporting cells in the goldfish sacculus. J Physiol. 1996; 495(Pt 3):665–679. [PubMed: 8887774]

Trapani JG, Nicholson T. Mechanism of spontaneous activity in afferent neurons of the zebrafish lateral line organ. J Neurosci. 2011; 31:1614–1623. [PubMed: 21289170]

Wainger BJ, DeGennar M, Santoro B, Siegelbaum SA, Tibbs GR. Molecular mechanism of cAMP modulation of HCN pacemaker channels. Nature. 2001; 411:805–810. [PubMed: 11459060]

Wahl-Schott C, Biel M. HCN channels: structure, cellular regulation and physiological function. Cell Mol Life Sci. 2009; 66:470–494. [PubMed: 18953682]

Wooltorton JR, Gaboyard S, Hurley KM, Price SD, Garcia JL, Zhong M, Lysakowski A, Eatock RA. Developmental changes in two voltage-dependent sodium currents in utricular hair cells. J Neurophysiol. 2007; 97:1684–1704. [PubMed: 17065252]

Yi E, Roux I, Glowatzki E. Dendritic HCN channels shape excitatory postsynaptic potentials at the inner hair cell afferent synapse in the mammalian cochlea. J Neurophysiol. 103:2532–2543. [PubMed: 20220080]

Zhang R, Haverich A, Struber M, Simon A, Pichlmaier M, Bara C. Effects of ivabradine on allograft function and exercise performance in heart transplant recipients with permanent sinus tachycardia. Clin Res Cardiol. 2008; 97:811–819. [PubMed: 18648727]

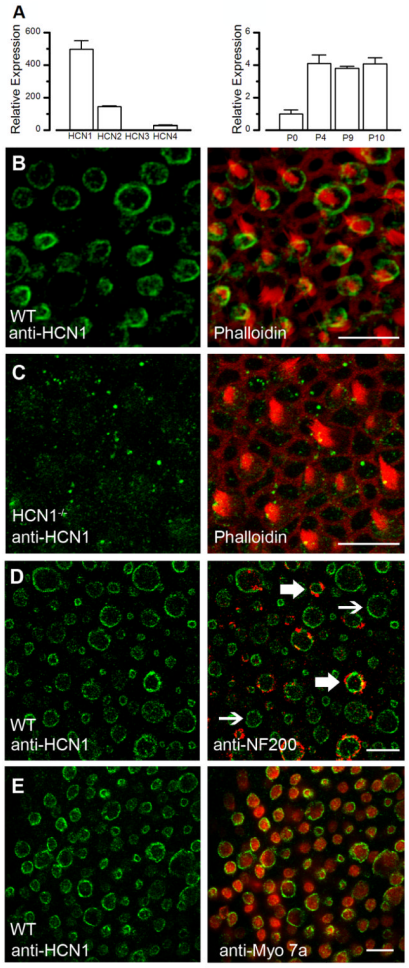

Figure 1.

Expression of HCN subunits in the mammalian utricle. ***A,*** Quantitative RT-PCR was used to estimate mRNA copy number for each of the four *Hcn* genes from a pool of 10 utricles collected at postnatal day (P) 8 (left). Data were normalized to *Hcn3* mRNA expression. Relative expression of *Hcn1* mRNA normalized to 29S and the P0 sample from a pool of 10 utricles collected at four different developmental time points (right). Error bars represent standard error of the mean from three replicates. ***B,*** HCN1 in the basolateral hair cell membrane of a mouse utricle (green). Phalloidin (red) is shown in a merged image on the right. The projection of several focal planes through the utricle epithelium reveals that HCN1 is visible in nearly every hair cell basolateral membrane and absent from stereocilia. Scale bar = 10 μm. ***C,*** HCN1 staining (green) of an Hcn1-deficient mouse utricle. Phalloidin (red) is shown in a merged image on the right. Scale bar = 10 μm. ***D,*** HCN1 in the basolateral hair cell membrane of a mouse utricle (green) counterstained with neurofilmanet-200 (red) to identify afferent terminals. Thin arrows indicate hair cells positive for HCN1 with no visible neurofilament staining, indicating probable type II hair cells. Thick arrows indicate probable type I hair cells positive for HCN1 and surrounded by calyx afferents. Scale bar = 10 μm. ***E,*** Confocal image of wild-type mouse utricle hair cells stained with HCN1 (green) and myosin 7a (red). Nearly 90% of hair cells showed HCN1 expression. Scale bar = 10 μm.

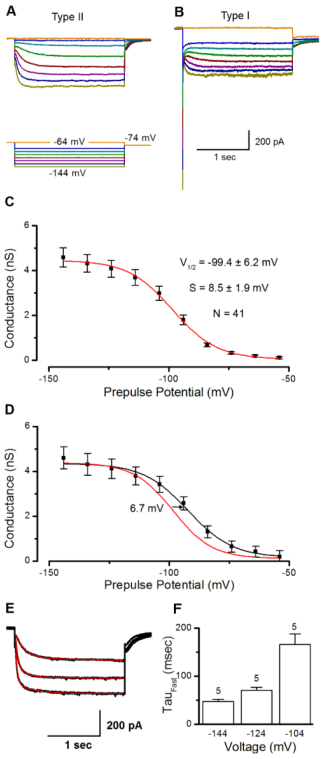

Figure 2.

I_h in wild-type vestibular hair cells. Representative traces showing voltage-dependent currents through HCN channels in P8-10 mouse utricular hair cells. Currents were evoked with voltage steps between −144 mV and −64 mV from a resting potential of −64 mV using the protocol shown below panel *A*. ***A, B,*** Representative wild-type currents measured from a type II (*A*) and type I (*B*) hair cell. Note the large, slowly activating inward current typical of I_h. In panel *B*, $I_{K,L}$ active at rest is evident as a standing outward current and the large, fast inward current that deactivates at negative potentials. ***C,*** Activation curve generated from 41 type II hair cells. Tail currents were measured at −74 mV to eliminate contamination from I_{K1} and converted to conductance by dividing by driving force (30 mV). The data were fitted with a Boltzmann function (red line). ***D,*** Activation curve generated from 9 type II hair cells in the presence of 200μM 8-Br-cAMP. Data were fitted with a Boltzmann function (black line). The Boltzmann curve from Figure *2C* is replotted to facilitate comparison. ***E,*** Current evoked by steps to −144, −124, and −104 mV in a type II hair cell. Current amplitudes were normalized to facilitate comparison of activation kinetics. Red lines are double exponential fits of the currents. Currents were measured in the presence of Ba^{2+} in order to minimize the effect of the fast inward rectifier, I_{K1}. Mean fast time constants of activation for five cells are shown in ***F***.

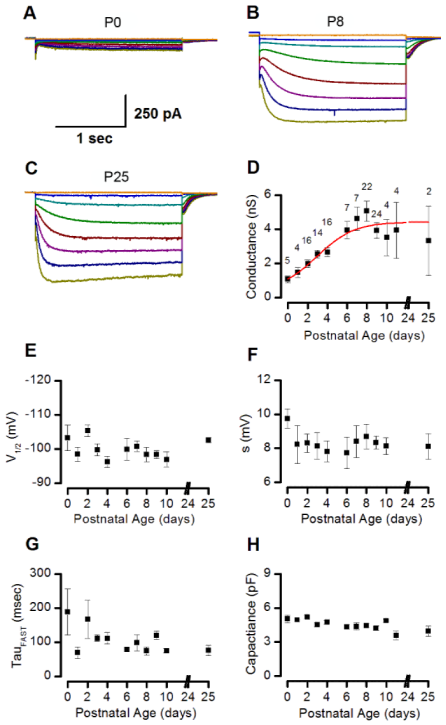

Figure 3.

Age-dependent acquisition of I_h. ***A, B, C,*** Representative families of currents acquired from type II hair cells at P0, P8, and P25, respectively. Note the increase in I_h between P0 and P8. Currents recorded at P25 resembled those found at P8. ***D,*** Plot of mean maximal conductance from type I and type II hair cells versus postnatal age. Conductance increased throughout the first postnatal week and reached a plateau beginning around P8. ***E, F, G,*** Half-activation potential, slope factor (s), and activation kinetics, respectively, from type II hair cells, plotted as a function of postnatal age. ***H,*** Whole-cell capacitance from both type I and type II hair cells plotted as a function of postnatal age. Number of samples at each developmental stage were: P0=5;, P1=4, P2=16, P3=14, P4=16, P6=7, P7=7, P8=22, P9=24, P10=4, P11=4, and P25=2.

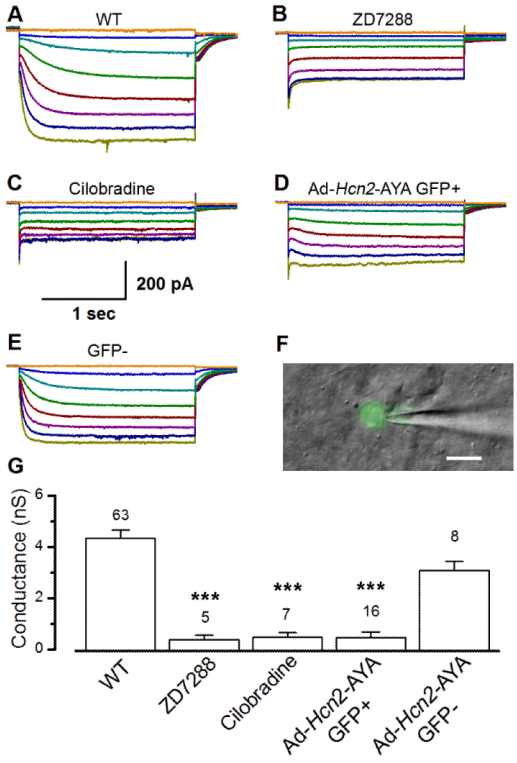

Figure 4.

Inhibition of I_h in vestibular hair cells. ***A,*** A representative family of traces from a wild-type vestibular hair cell. ***B, C,*** Representative families of currents from wild-type cells after application of 100 μM ZD7288 (*B*) or 10 μM Cilobradine (*C*). While the fast inward rectifier I_{K1} remained, I_h was completely blocked in both cases. ***D,*** A representative family of currents from a GFP-positive cell with residual I_h after transfection with the HCN2-AYA construct. In 12 of 16 cells, I_h was completely absent and the currents resembled those seen in *B* and *C*. In the remaining 4 cells, the current was significantly reduced. ***E,*** Representative currents from a neighboring GFP-negative cell. The cell was not transfected and the currents resembled those recorded from wild-type controls, as shown in panel *A*. ***F,*** DIC image of a GFP-positive cell. Scale bar = 10 μm. ***G,*** Bar graph summarizing the conductance values from 63 wild-type cells, 5 cells after application of ZD7288, 7 cells after application of Cilobradine, 16 cells GFP-positive for HCN2-AYA, and 8 GFP-negative cells. Asterisks mark statistically significant differences ($p<0.001$) relative to wild-type (WT).

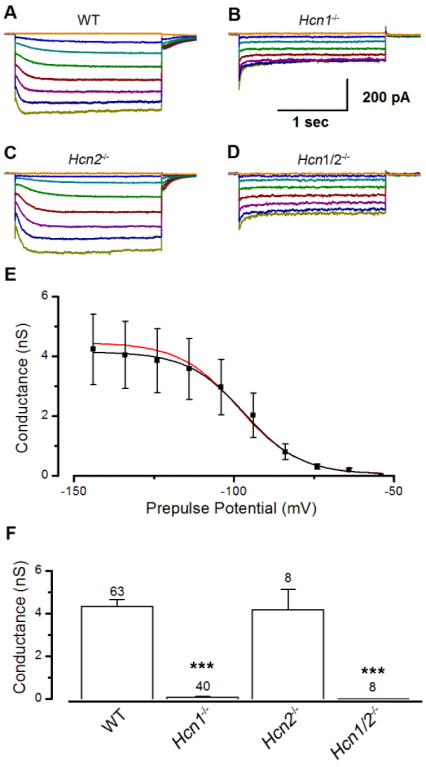

Figure 5.

I_h in vestibular hair cells of *Hcn*-deficient mice. Representative traces showing voltage-dependent currents in P8-10 type II mouse utricular hair cells lacking *HCN1, 2,* or both. Currents were evoked using the same voltage protocol shown in Figure 3. ***A,*** Representative traces from a wild-type type II hair cell. ***B, C, D,*** Representative traces from an HCN1, HCN2, and HCN1/2-deficient hair cell respectively. Note the complete loss of I_h in both the HCN1 and HCN1/2-deficient cells. Currents recorded from HCN2-deficient hair cells resembled those recorded from wild-type tissue. ***E,*** Activation curve from HCN2-deficient hair cells. Data from 8 cells were averaged and fitted with a Boltzmann equation (black line). For comparison, the same Boltzmann curve used to fit the WT data of Fig. 2*C* is reprinted (red line). ***F,*** Summary of maximum conductance for 63 wild-type, 40 $HCN1^{-/-}$, 8 $HCN2^{-/-}$, and 8 $HCN1/2^{-/-}$ cells. Asterisks mark statistically significant differences ($p<0.001$) relative to WT.

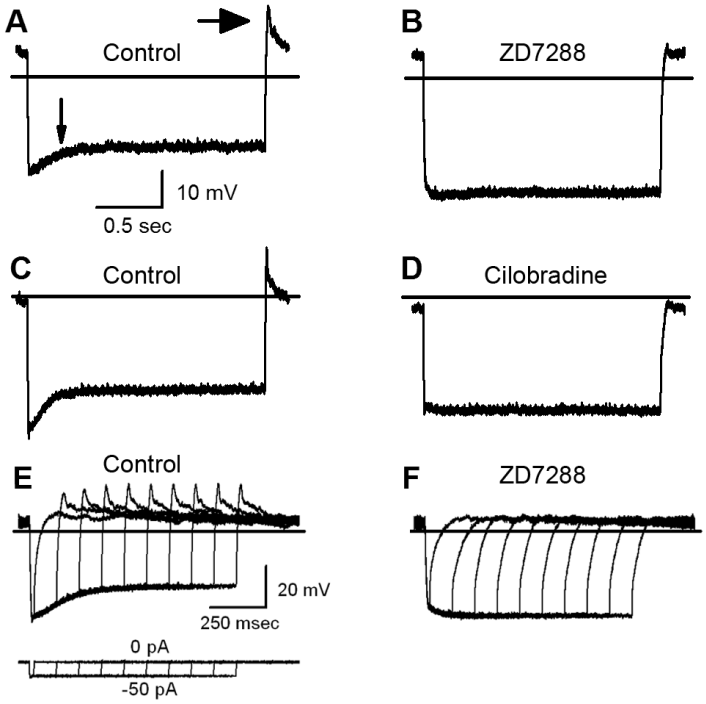

Figure 6.

Hair cell voltage responses. Hair cell voltage responses were measured in current-clamp mode. Two-second current steps of 50 pA or less (panels *A-D*) were used to hyperpolarize the cell to ~ −90 mV. The horizontal lines indicate −60 mV. The scale bars apply to panels *A-D*. ***A,*** Representative response from a type II hair cell of a wild-type mouse utricle at P8. Following the initial hyperpolarization, the cell depolarized to a steady state level. The depolarizing sag is indicated by a small arrow. When the current was stepped back to 0 pA, the voltage rebounded with a peak near −40 mV (large arrow). ***B,*** The same cell shown in *A* after application of 100 μM ZD7288. ***C,*** Other representative wild-type voltage responses before and after (***D***) application of 10 μM Cilobradine. ***E,*** A family of representative voltage responses recorded from a type II hair cell at P7. The responses were evoked by the current protocol shown below. The scale bars apply to panels *E-F*. ***F***, The same cell shown in *E* after application of 200 μM ZD7288 and full block of I_h.

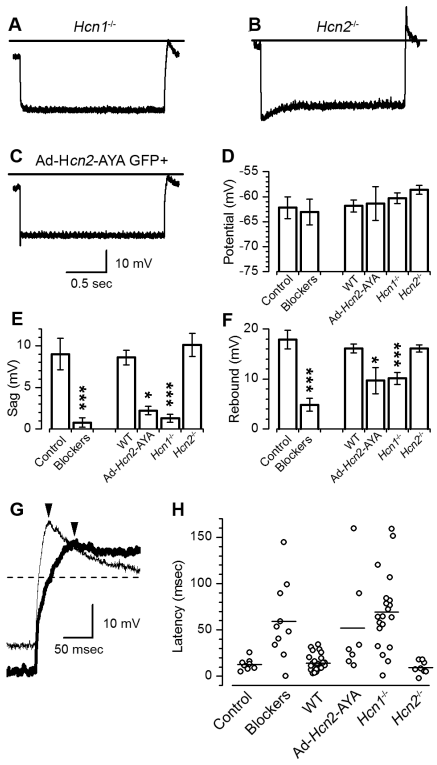

Figure 7.

Functional contributions of I_h. ***A***, Representative voltage response from an *Hcn1*-deficient cell, again demonstrating a loss of the sag and the rebound potentials. ***B,*** Voltage response of an *Hcn2*-deficient cell, demonstrating normal sag and rebound potentials. ***C,*** Voltage response from an HCN2-AYA transfected cell demonstrating the loss of I_h. The scale bars apply to panels *A*-*C* and the horizontal lines indicate −60 mV**. *D*-*F,*** Mean values taken from current-clamp measurements of resting potential ***(D)***, the sag potential (***E)*** and the rebound potential (***F)***. **Figure 7.** Function contributions of I_h. A representative voltage response from an *Hcn1*-deficient cell, again demonstrating a loss of the sag and the rebound potentials. ***A,*** Voltage response of an *Hcn2*-deficient cell, demonstrating normal sag and rebound potentials. ***B,*** Voltage response from an HCN2-AYA transfected cell demonstrating the loss of I_h. ***C*-*E,*** Mean values taken from current-clamp measurements of resting potential ***(C)***, the sag potential (***D)*** and the rebound potential (***E)***. Resting potential was measured from the first 50 data points at the beginning of the trace with current clamped at 0 pA. The sag potential was measured as the difference between the peak hyperpolarization and steady-state hyperpolarization near the end of the current step. The rebound was measured as the difference between resting potential and the peak depolarization at the end of the step. Mean values were measured as the average from 8 control cells and the same 8 cells following exposure to either 100 μM ZD7288 or 10 μM Cilobradine, 25 wild-type cells, 5 cells exposed to the HCN2-AYA construct, 20 cells from *Hcn1*-deficient mice and 7 cells from *Hcn2*-deficient mice. Asterisks indicate statistically significant differences (*: $p<0.05$; ***: $p<0.001$) relative to WT. ***G,*** Magnified view of two representative rebound potentials. Trace from a wild-type cell (thin line) and an *Hcn1* knockout cell (thick line) are shown. Arrowheads mark the peak rebound potentials. ***H,*** Scatter plot showing latency measured as the temporal difference between the end of the step and the peak rebound potential. Solid lines represent means. The variability in control, wild-type, and *Hcn2*- deficient cells was

minimal, while cells exposed to blockers, dominant-negative constructs, or cells deficient in *Hcn1* showed considerable variation.

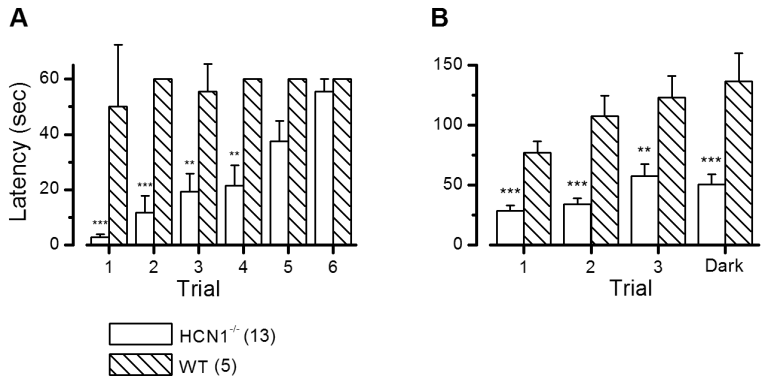

Figure 8.

Rotarod performance of wild-type and *Hcn1*$^{-/-}$ mice. 18 mice (5 wild-type and 13 *Hcn1*$^{-/-}$) were tested for balance deficits using the rotarod apparatus. Mice were tested between 1.5 and 2 months of age. ***A,*** Time to fall during training on a stationary rod. Naïve wild-type mice showed little difficulty with this task, while *Hcn1*-deficient mice required multiple trials before demonstrating the ability to remain on the stationary rod. ***B,*** Time spent on the rotarod apparatus accelerating at 0.1 RPM/s from a starting speed of 2RPM. *Hcn1*-deficient mice fell significantly earlier than wild-type controls on each of the three trials. Trial 4 indicates a dark trial in which the lights were turned off in order to limit visual compensation. Statistically significant differences are marked with asterisks.

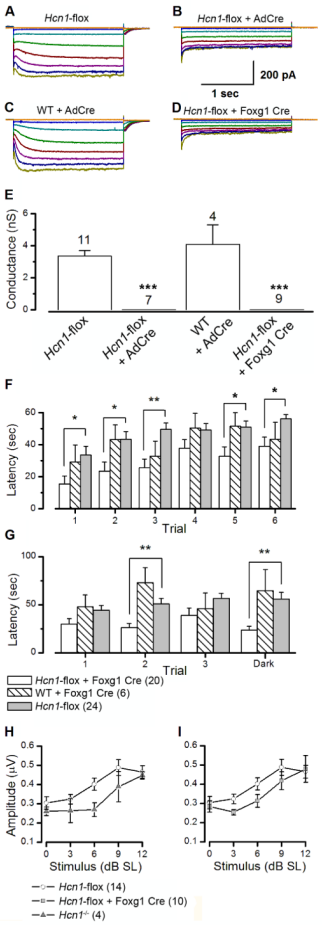

Figure 9.

Conditional knockout of *Hcn1*. ***A,*** Representative currents recorded from an *Hcn1*-floxed vestibular hair cell negative for GFP and Cre-recombinase. ***B,*** Currents recorded from an *Hcn1*-floxed hair cell positive for GFP and Cre-recombinase after transfection with an Ad-Cre-GFP. Note the complete lack of I_h, which resembles currents from *Hcn1* deficient mice shown in Fig. 5*B*. ***C,*** I_h recorded from a wild-type GFP-positive hair cell transfected with Ad-Cre-GFP. ***D***, Representative currents from a mouse with hair cell deletion of *Hcn1* through expression of *Foxg1 Cre-recombinase*. Note the complete lack of I_h, similar to panel *B* and to *Hcn1*-deficient tissue. ***E,*** Mean maximum conductance from 11 *Hcn1*-floxed cells, 7 *Hcn1*-floxed cells infected with AdCre-GFP, 4 wild-type cells infected with AdCre-GFP, and 9 *Hcn1*-floxed cells expressing Cre under the Foxg1 promoter. Asterisks mark statistically significant differences ($p<0.001$) relative to *Hcn1*-floxed hair cells. ***F,*** Rotarod performance in 6 training trials of 20 conditional *Hcn1* knockout mice (white bars), six mice positive for *Foxg1-Cre* (striped bars), and 24 *Hcn1*-floxed mice without Cre expression (gray bars). Mice were approximately 4 to 6 months old. Asterisks indicate statistically significant differences (*: $p<0.05$; **: $p<0.005$) between the *Hcn1*-floxed group and the *Hcn1*-floxed mice heterozygous for *Foxg1-Cre*. ***G,*** Performance of conditional *Hcn1* knockouts on accelerating testing tasks was also significantly worse in two of the four trials than mice with floxed alleles but no Cre-recombinase. ***H, I,*** Peak-to-peak amplitude measurements of vestibular evoked potentials in three genotypes of mice. Amplitudes reported represented the difference in the first positive and first negative peak in the recorded waveform. Data were normalized to 0 dB SL which represented the threshold

response. We noted a significant decrease in amplitude at 6 dB SL between the 14 *Hcn1*-floxed mice (white circles) and the 4 global *Hcn1*-deficient mice (gray triangles, *H*). There was also a significant decrease in amplitude at the 3 and 6 dB SL between 14 *Hcn1*-floxed mice (white circles) and the 10 Cre-positive *Hcn1*-floxed mice (gray squares, *I*).